JTTEE5 20:317–327
DOI: 10.1007/s11666-010-9567-z
1059-9630/$19.00 © ASM International

Analysis of the Mechanical Properties of an Arc Sprayed WC-FeCSiMn Coating: Compression, Bending, and Tension Behavior

W. Tillmann and J. Nebel

(Submitted April 29, 2010; in revised form September 12, 2010)

This paper is concerned with the elastic and plastic forming behavior of arc sprayed WC-FeCSiMn coatings. The mechanical properties were investigated by indentation, bending, and tensile tests. These were performed on coated mild steel substrates as well as spark eroded and ground freestanding coatings with different geometries. The results of the indentation, bending, and tensile tests were evaluated concerning the coating microstructure, element, and pore distribution, as well as the local microhardness. The critical role of pores and inhomogeneities within the sprayed coating was examined in detail. Micro- and macrocracking were investigated by scanning electron microscopy after the indentation and tensile tests. It was figured out that the WC-FeCSiMn coating featured a distinctive brittle behavior. During the bending and tension tests, brittle forced fracture of the layer appeared almost without plastic deformations. A significant difference was determined between the compression and tensile performance of the coating. For instance, the Young's modulus for compression strains was measured to be approximately 60% higher than the tension case.

Keywords arc spraying, bending test, hardness, nanoindentation, porosity, tensile test

1. Introduction

Because of their high hardness and toughness, WC-based cermet coatings have been used for wear-resistance applications for many decades. Milling heads, crushers, and conveyor systems in the construction, stone, agriculture, and waste disposal industries are typical examples that have been improved by this kind of coating (Ref 1-4).

Correlating with the industrial acceptance of WC cermet coatings the application areas are currently continuously expanding. New devices such as landing gears, hydraulic seals, or cylinder surfaces in high-pressure applications characteristically show a higher tribological complexity and require advanced accuracy and reliability (Ref 3, 5). In particular, features such as stiffness, strength, and crack resistance of the coating are of particular interest (Ref 6).

However, the identification of these mechanical coating properties such as hardness, bending strength, fracture toughness, and Young's modulus are challenging because of the inhomogeneity and anisotropy of the layer. The typical lamellar microstructure with ''pancake'' splats, horizontal and vertical microcracks, pores, and weak interlamellar cohesion (Ref 7-9) do not only cause difficulties for the measurement, but also tend to result in large deviations and errors. In particular, since the coating is a composite material, the mechanical behavior is certainly different from that of a bulk homogeneous material (Ref 8, 9).

In the past, much research was conducted considering the mechanical properties as well as the elastic and plastic forming behavior of thermal sprayed coatings. However, there is still a lack of validated tests, experimental benchmarks, and available databases of coating properties for calculations and simulations.

The easiest standardized methods to gain comparable mechanical properties of a coating are the indentation tests (Ref 10). Vickers, Brinell, and Rockwell tests are used to determine the hardness and, if applicable, the cracking resistance of the sprayed layer (Ref 8, 9). Since they are easy to use, fast, and reliable, they are crucial elements of coating research and development. On the other hand, the informative value of a hardness measurement is rather poor. The indentation tests are mainly valid as a first indicator of the coating behavior under compressive loads such as the forming behavior and crack propagation. The fracture toughness (K_{IC}) and the resistance against abrasive wear can be roughly estimated (Ref 8, 9, 11-15).

This article is an invited paper selected from presentations at the 2010 International Thermal Spray Conference and has been expanded from the original presentation. It is simultaneously published in *Thermal Spray: Global Solutions for Future Applications, Proceedings of the 2010 International Thermal Spray Conference,* Singapore, May 3-5, 2010, Basil R. Marple, Arvind Agarwal, Margaret M. Hyland, Yuk-Chiu Lau, Chang-Jiu Li, Rogerio S. Lima, and Ghislain Montavon, Ed., ASM International, Materials Park, OH, 2011.

W. Tillmann and **J. Nebel**, Institute of Materials Engineering, TU Dortmund, Dortmund, Germany. Contact e-mails: jan.nebel@udo.edu and wolfgang.tillmann@udo.edu.

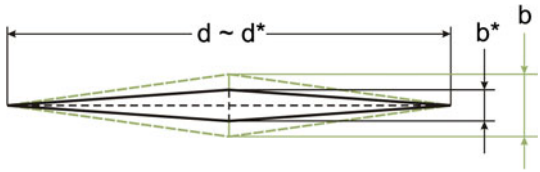

Fig. 1 Young's modulus estimation by Knoop indentation

Knoop indentation tests further enable the evaluation of the Young's modulus based on a model comparing the elastic recovery of indenter impressions with the original dimensions of the Knoop indenter geometry (Fig. 1) (Ref 9, 15-19).

Based on the relation of Marshall et al. (Ref 19):

$$\frac{b^*}{d^*} \approx \frac{b^*}{d} = \frac{b}{d} - \frac{0.45H}{E} \qquad \text{(Eq 1)}$$

the Youngs modulus can be determined correlating to the characteristic elastic recovery in the b direction. Where E is the Young's modulus, H is the Knoop hardness, b and d are the diagonals of the Knoop indenter geometry, and b^* and d^* are the diagonals of the indenter impression (Ref 19). The length of the impressions of major diagonal d remains relatively unaffected and is negligible (Fig. 1).

A more precise way to investigate the modulus of elasticity is given by indentation test setups with continuous recording of load and indentation depth. Entire compressive stress-strain curves can be determined including elastic, plastic, and creep behavior. The best-known depth-sensing method is the nanoindentation test, using a Berkovich indenter (Ref 9, 10, 20-29). This technique relies on a high-resolution load and displacement measurement of the three-sided precision pyramid indenter. Based on the model of Oliver-Pharr (Ref 22), the Young's modulus can be calculated from the slope of the unloading curve progression.

However, the characterization of inhomogeneous materials such as thermally sprayed coatings is nontrivial. Only local properties at a certain surface area can be investigated. These local features have to be identified for each material phase in a number of nanoindentation experiments. Mechanical properties for the entire material can only be approximated. Additionally, there is a characteristic difference between the compressive and tensile behavior for brittle materials. For instance, the tensile strength of ceramics and cermets are characteristically lower than their compressive strength (Ref 20, 30, 31). Typically, thermally sprayed coatings also feature a rather brittle behavior at tensile loads. These characteristics derive from the inhomogeneous microstructure. Surface roughness, microcracks, pores, oxides, hard phases, and weak splat-to-splat interfaces within the coating lead to strain localizations and decrease the Young's modulus, ultimate strength, durability, and ductility (Ref 20, 32-34). Combined with residual stresses in the coating, these integrated notches promote the crack initiation and propagation (Ref 6, 35).

Compared with indentation test methods, tensile tests can be used to evaluate the stress-strain behavior under tension loads. However, it is rather difficult to prepare suitable samples for testing (Ref 36, 37).

Only a few publications are available concerning tensile tests on thermal sprayed coatings. Additionally, the reported research was mainly examined on coated steel composites with limited validity because of an unknown interaction of coating, interface, and substrate (Ref 33, 38). To ensure meaningful results, freestanding coatings of defined geometries and with a low surface roughness need to be produced without inducing additional stresses during the machining process (Ref 36), which complicates the sample preparation process.

Considering the characteristic of brittle materials that the tensile strength is lower than the compressive strength, bending tests can be used to determine the Young's modulus and strength in the direction of the tension as well. This is possible, since the deformation and fracture initiation are mainly attributed to the tensile strains.

Because the preparation of the specimen is less complex, bending tests are more popular than tensile tests (Ref 6, 7, 20, 32, 35, 39). However, as mentioned previously, the preparation of freestanding coatings with low surface roughness is necessary to calculate authentic mechanical values for the sprayed layer.

The research objective of this study is the investigation of mechanical properties of arc sprayed WC-FeCSiMn coatings. Conducting different indentation, bending, and tensile tests the coating performance is distinguished between compression and tensile strains.

Freestanding coatings and coated steel samples are used for testing to analyze the interaction effect between substrate, coating, and interface on the validity of the experimental data.

2. Experimental

2.1 TWAS Spraying

A twin wire arc spraying (TWAS) facility (Smart Arc PPT 350, Sulzer Metco, Switzerland) was used to spray WC-FeCSiMn coatings. The work principle of the spraying process used in this research work is described elsewhere (Ref 40-42).

The wire feedstock material used was a Duramat AS 850 flux-cored wire with a diameter of 1.6 mm (Durum GmbH, Germany). The wire is a Fe-based alloyed with 2% C, 1.4% Si, and <1% Mn. It is filled with 50 wt.% of fused tungsten carbide (WC/W_2C) with grain sizes of 25-125 μm.

In preparation for thermal spray experiments, all substrates were grit blasted with coarse-grained EKF 24 alumina (710-850 μm). A pressure of 2 bar, an inclination angle of 70° and a stand-off distance of 100 mm were chosen as grit-blasting parameters. After the blasting procedure, the substrate surface showed an average roughness of $R_z = 39 \pm 4$ μm; $R_a = 5.5 \pm 0.6$ μm. Subsequently, the samples were cleaned for 15 min in an ethanol

Table 1 Spray parameters of WC-FeCSiMn

Primary gas pressure, bar	Arc voltage, V	Arc current, A	Stand-off distance, mm	Jet velocity, mm/min
6	30	220	100	12,000

ultrasonic bath and heated to approximately 100 °C in a convection furnace for about 30 min to reduce the thermal stresses during the coating process.

The coating parameters for the TWAS spraying of WC-FeCSiMn are based on the parameter optimization presented in Ref 42. Table 1 summarizes the selected optimized spraying parameters used in this paper.

Medium-carbon steel specimens (Mat. No. 1.0503, DIN C45, AISI 1045) were chosen as substrates. Related to the required test geometries for the indentation, bending, and tension experiments, different specimen dimensions were coated by arc spraying. However, there were two fundamentally different procedures to manufacture coated and freestanding specimens.

To generate WC-FeCSiMn-coated steel specimens, the preparation of the substrate was adapted to the final test geometry. Rectangular mild steel samples with a dimension of 70 × 50 × 10 mm were used as substrates for the indentation test. Form A.1 steel specimens (Ref 37) with $L_t = 150$ mm, $L_0 = 50$ mm, $a_0 = 3$ mm, and $b_0 = 12.5$ mm were chosen as substrate geometry for the bending tests (Ref 38) and the tensile testing (Ref 37). They were arc sprayed with WC-FeCSiMn layers of ~450 μm and ground to a thickness of ~340 μm. In contrast to the bending test samples, the tension test specimens were coated on both sides to approximate an axial symmetric stress condition during the tension experiment.

The freestanding WC-FeCSiMn coatings were machined out of coated 250 × 150 × 10 mm mild steel plates with an initial coating thickness of ~2.2 mm by eroding and grinding processes according to DIN EN ISO 843 (Ref 36). Form A.1 steel specimens (Ref 37) with $L_t = 120$ mm, $L_0 = 50$ mm, $a_0 = 1.5 \pm 0.02$ mm, and $b_0 = 9.0 \pm 0.02$ mm were prepared for the tensile tests and rectangular specimens with the dimension of 60 × 9.0 × 1.5 ± 0.02 mm for the bending tests.

2.2 Microstructural Analytics

The layer morphology of the thermal sprayed specimens was investigated by light microscopy (Axiophot, Zeiss, Jena, Germany) on polished cross sections. Additionally, the coating microstructure, nanoindentation, and Vickers hardness imprints and fracture pattern were investigated in higher magnification using scanning electron microscopy (SEM) (JSM-7001F, FEM Jeol, Eching, Germany). EDS measurements (INCA x-act, Oxford Instruments, Wiesbaden, Germany) were used to characterize the chemical composition of the sprayed layers.

Porosity measurements of the coatings were performed with the commercial image analysis software (Axiovision 4.63, Zeiss, Jena, Germany) on 10 cross-section pictures taken at 200× magnification by light microscopy. The results were validated by image analysis measurements on 10 SEM pictures (magnification 300×) with the Axiovision software (Zeiss, Jena, Germany) as well as the Grainplot image analyzing tool (Institute of Mechanics, Dortmund, Germany).

2.3 Residual Stress Measurement

The hole-drilling method was used to determine the residual stress depth profile of the investigated layers. According to the ASTM Standard E837 (Ref 43), a high-speed air turbine drill was used to remove coating material in the center of a rosette strain gage. At each depth increment, the strain relief on each of the gages was measured and the stress distribution was estimated. To achieve valuable results, the residual stress measurements were conducted at machined samples with test geometry (eroded and ground).

2.4 Indentation Tests

Hardness Vickers, Brinell, Rockwell tests were conducted on an universal hardness tester, (DIA-TESTOR 7521, Wolpert Hahnkolb, Stuttgart, Germany) according to DIN EN ISO 6506 (Ref 44), DIN EN ISO 6507 (Ref 45), DIN EN ISO 6508 (Ref 46), and VDI/VDE 2616 (Ref 47). To examine the coating microhardness (HV0.1, HV1) relating to DIN EN ISO 6507 (Ref 45) and DIN EN ISO 4516 (Ref 48) a M-400 microhardness tester (LECO, Germany) was used. The nanoindentation experiments were performed at the Institute of Materials, Ruhr University Bochum using an encapsulated Nanoindenter XP equipment (MTS Nano Instruments, Oak Ridge, TN).

To generate representative hardness and Young's modulus values, 10 imprints were investigated for the HRC, HV30, and HBW measurements, respectively. Thirty imprints were examined for the HV1 and HV0.1 experiments at the polished coating surface as well as at the cross section, and 49 imprints were analyzed for each nanoindentation test with indentation depths of 100, 250, and 500 nm.

In addition to the standardized indentation methods described previously, a customized setup proved to characterize the nature of thermally sprayed coatings elasticity, durability, and cracking under high loading pressures. Based on the results of Lawn (Ref 49), who analyzed the mechanics of plastic deformation and damage mechanisms of ceramics induced by spherical indentation, and the results of Marshall et al. (Ref 19) and Herbert et al. (Ref 21), who determined the Young's modulus by elastic recovery measurements of diverse indenter impressions, a spherical indenter test was taken into consideration. Figure 2 illustrates the principle of the investigated indentation test.

Assuming one-directional springback in spherical indentation experiments, it was aspired to figure out the elastic and plastic deformation ratio, to develop a model to reproduce the indentation experiment, and to calculate the compressive strength and Young's modulus of the coating. The main advantage of spherical indenter

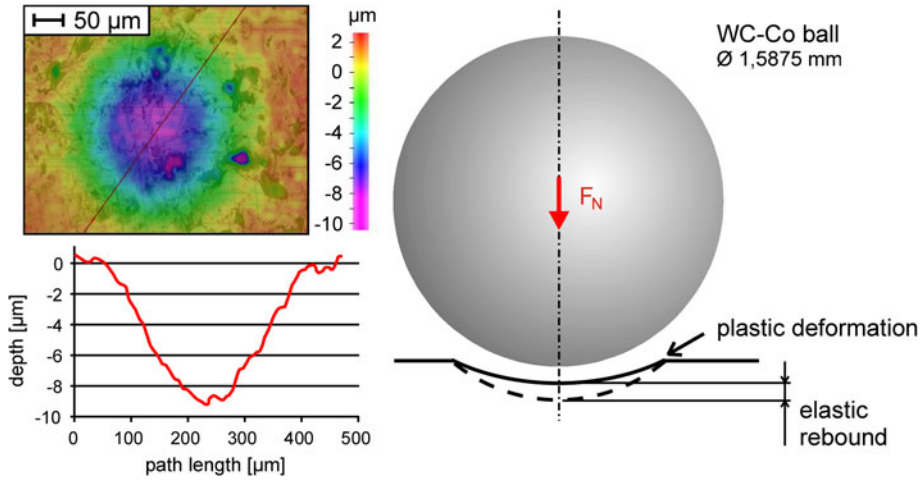

Fig. 2 Concept draft to determine mechanical and damage characteristics of thermal sprayed coatings by spherical indentation

geometry was expected to be an easier modeling of the rotationally symmetrical indentation experiment compared with Knoop and Vickers hardness tests. Additionally, the spherical geometry shows a larger indentation surface to depth aspect ratio that should allow the investigation of relatively thin and inhomogeneous coatings.

The spherical indentations were realized on a DIA-TESTOR 7521 universal hardness tester (Wolpert Hahnkolb, Stuttgart, Germany) according to DIN EN ISO 6506 (Ref 44) and VDI/VDE 2616 (Ref 47). The coating surface was ground and polished previously. The indenter impressions were measured employing three-dimensional (3D) optical microscopy (IFM-G3, Alicona Imaging GmbH, Switzerland). The theoretical indentation depth h_i including the plastic and elastic impression of the spherical indenter was calculated correlating the measured indentation width d_i with the original WC-Co ball dimension D_i:

$$h_i = \frac{D_i}{2}\left(1 - \sqrt{1 - d_i^2/D_i^2}\right) \quad \text{(Eq 2)}$$

2.5 Bending Test

The bending behavior of the coating was analyzed by a three-point bending test setup with an in situ 3D optical measurement (IFM-G3, Alicona Imaging GmbH, Switzerland) of the bending radius and in situ observation of the bending forces using strain gauges. The customized test setup is shown in Fig. 3.

The bending stress in the outer fibers at the midpoint σ_f and strain in the outer surface of the tested sample ε_f and the Young's modulus E were calculated by:

$$\sigma_f = \frac{3Fl}{2bh^2} \quad \text{(Eq 3)}$$

$$\varepsilon_f = \frac{6dh}{l^2} \quad \text{(Eq 4)}$$

$$E = \frac{\Delta F l^3}{4bh^3 \Delta d} \quad \text{(Eq 5)}$$

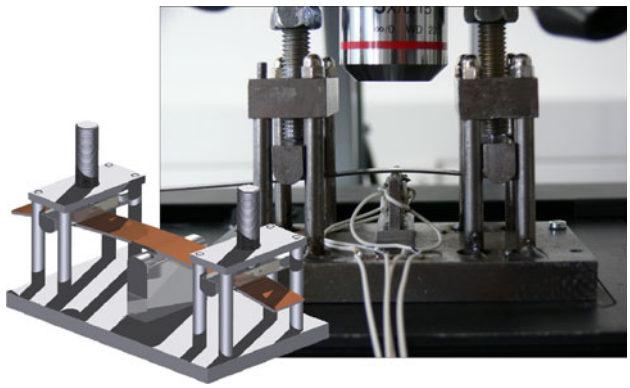

Fig. 3 Bending test setup

where F is the applied load, l is the distance between the two outer spans (here, 41.5 mm), b is the sample width, h is the sample thickness, and d is the deflection at middle span (Fig. 4).

2.6 Tensile Tests

According to DIN EN ISO 6892 (Ref 37), the tensile tests were conducted with a hydraulic tension-compression fatigue tester (Instron type 8800, Instron Limited, High Wycombe, England). The tensile stress was calculated by:

$$\sigma = \frac{F}{bh} \quad \text{(Eq 6)}$$

while the ultimate strength σ_{max} was determined for the maximum force, applied before the first coating fractures were visible.

The Young's modulus was computed using Eq 6 and 7 in the elastic range of the stress-strain ratio where Hooke's Law holds.

$$E = \frac{\sigma}{\varepsilon} \quad \text{with} \quad \varepsilon = \frac{\Delta l}{l_0} \quad \text{(Eq 7)}$$

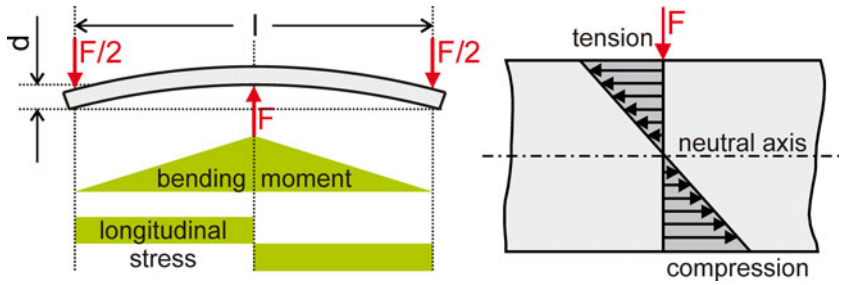

Fig. 4 Young's modulus estimation by three-point bending

Mean values of the ultimate strength and Young's modulus were estimated for 10 WC-FeCSiMn coated steel samples with a coating thickness of 340 µm on both sides as well as three freestanding coatings of 1500 µm.

The fracture patterns of arc sprayed steel samples and freestanding coatings were investigated by SEM.

3. Results and Discussion

3.1 Coating Microstructure

The microstructure of the sprayed WC-FeCSiMn coating shows the typical inhomogeneous lamellar structure of an arc sprayed layer. ''Pancake'' splats of irregular shape and chemical composition are visible in the SEM cross sections (Fig. 5). Related to the intensity of the backscattered electrons (BSE), the brightness of the grayscale illustrates the element distribution qualitatively. Elements with high atomic weight appear brighter than lighter elements. Correlating with the huge difference in the relative atomic weight of tungsten (183.84 g/mol) and iron (55.845 g/mol), the phases of the sprayed WC-FeCSiMn feature a good contrast. In addition to these two phases, many pseudoalloyed splats containing WC as well as FeCSiMn are visible. However, an accurate characterization of WC and W_2C phases is restricted by the low carbon EDS sensitivity.

Obviously horizontal and vertical microcracks are located in the hard WC/W_2C splats. Flat pores between the splats indicate a weak interlamellar cohesion. Round voids of different sizes are spread over all composite phases and between the splats. The porosity, including all pores, microcracks, and voids, was determined with three different image analysis methods. The results are given in Table 2.

Figure 6 illustrates the pore quantity, pore size distribution, and relative pore area related to the pore dimension cumulated over 10 cross sections taken by light microscopy at 200× magnification.

The diagram shows that the microstructure is characterized by numerous small pores with a cross-sectional area of less than 20 µm^2. Many of them are flat interlamellar pores, surrounding the splats (Fig. 6). Furthermore, a small amount of pores derive from cross-section preparation breakouts. Even with cautious diamond grinding and polishing processes, existing microcracks in the hard

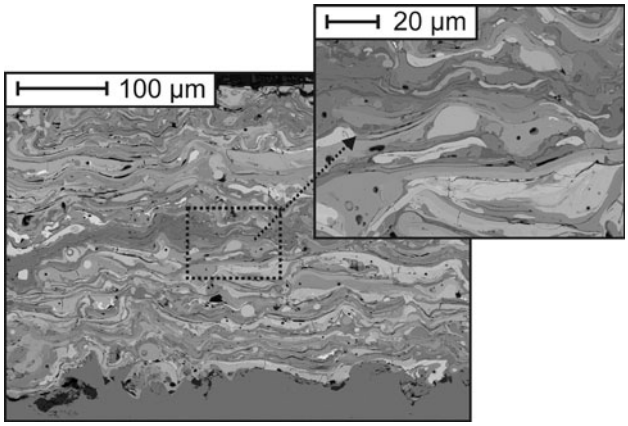

Fig. 5 SEM micrographs of TWAS WC-FeCSiMn cross-section (BSE-mode)

Table 2 Porosity measurements

	Porosity, vol.%		
	Axiovision (optical microscopy)	Axiovision (SEM)	Grainplot (SEM)
Arithmetic mean	2.08	2.03	2.32
Deviation	0.75	0.72	0.40

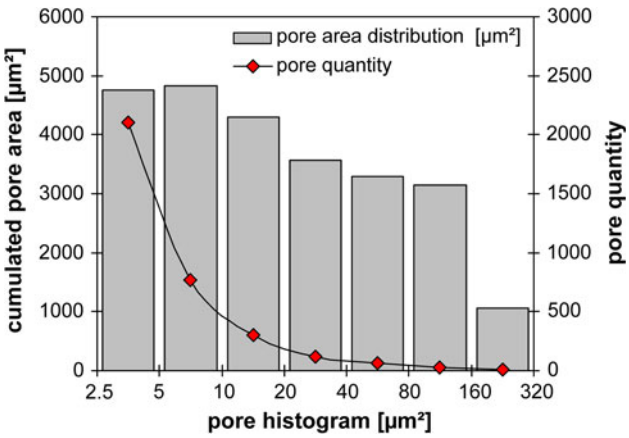

Fig. 6 Pore distribution concerning quantity, size, and dimension of the investigated WC-FeCSiMn coating

WC/W_2C phases can cause partial debonding of disconnected fragments.

3.2 Residual Stress

Residual stress measurements were conducted in order to support the discussion about the indentation, tensile, and bending tests. The residual stresses have a direct impact on the material properties, especially the yield strength, ultimate strength, and strain. The various examinations revealed residual tensile stresses in the arc sprayed WC-FeCSiMn layer, which derive from the solidification and cooling of molten droplets at their impact on the substrate. The highest residual tensile stress was detected at material composites of double-coated steel substrates. Figure 7 shows the depth profile of the residual tensile stress of a ground 340 µm WC-FeCSiMn layer on a substrate with a thickness of 3 mm.

The highest change in the residual tensile stress can be seen in the interface between the layer and the substrate. The residual tensile stress increases up to 120 MPa, closer to the layer surface. Freestanding eroded and ground layers, which were detached from the substrate, did not show these high residual tensile stress gradients. Although the layer thickness of 1500 µm was higher for the freestanding coatings than for the coated tensile specimens or bending specimens, the measured residual tensile stresses of the layer are lower and distributed more homogenously.

3.3 Indentation Tests

Numerous works have revealed that the hardness measured on the cross section of thermally sprayed coatings is characteristically higher than the hardness on the coating surface (Ref 7, 20). In the cross section, the ''pancake'' expansions of the splats perpendicular to the spray direction show a higher resistance to the indenter impression. Consequently, the hardness on the coating surface is reduced because of the thin lamellae and the weak interface between the splats.

Hence, the microstructural anisotropy of the layer in the investigated indentation tests was estimated for the coating surface and the cross section, respectively.

Table 3 contains the indentation test results including the hardness values and the compression Young's moduli referring to the indentation method and load.

It was noted that the indentation tests performed with high impression loads (HRC, HV30, HBW) resulted in low hardness values. Even the HV1 measurements showed a distinctly lower coating hardness when compared with the HV0.1 and nanoindentation experiments. This is due to the macroscopic expansion of the imprints and the energy dissipation during the partial cracking of the coating (Ref 12, 15). Elongated over many splats, pores, and splat boundaries the indenter takes advantage of these microstructural defects. This results in a reduced average hardness. Additionally, stress relaxation by cracking can be found far from the imprint. Furthermore, it has to be mentioned that the effect of the coating/substrate interface can not be neglected for the HRC, HV30, HBW1.5875/50, and HBW1.5875/40 measurements.

However, even with decreased indentation loads, all HBW measurements featured extreme low hardness values for the coating. Considering many indentation experiments and analytical investigations on the WC-FeCSiMn coating, as well as reference measurements on the bulk steel substrate, the effect that causes the low hardness values was identified. The analysis of the elastic and plastic deformation of the spherical indentation (illustrated in Fig. 2) shows a high divergence between the measured indentation depth and the calculated theoretical indentation depth (Eq 2). The divergence is visualized in Fig. 8.

Further investigations indicate that the TWAS coating spreads the pointed load of the spherical indenter to a wider area because of the layered lamellar structure. Like thin laminated springs the splats seemed to transmit the stress laterally toward the sides. Additionally, the round surface of the indenter entails a homogeneous stress distribution and reduces the notching effect at the indenter tip compared with, for example, the Vickers hardness pyramid. Whereas the measured indentation imprints showed realistic depths for each load, the width was significantly elongated. Because of this unexpected effect, the evaluation of the coating compressive strength and Young's modulus according to Fig. 2 was not possible.

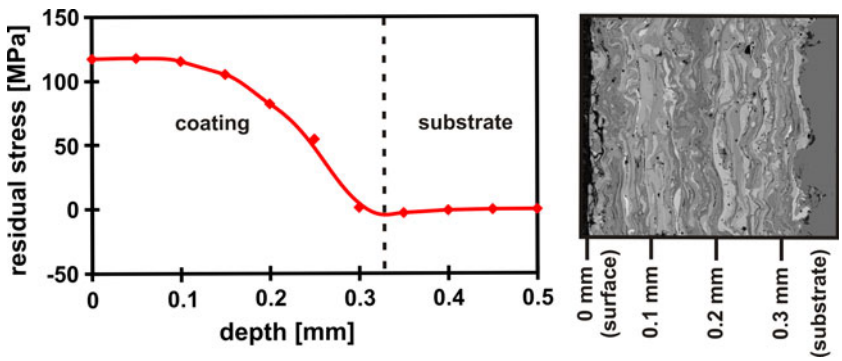

Fig. 7 Residual stress distribution in an arc sprayed WC-FeCSiMn coating on steel substrate (depth profile after grinding)

Table 3 WC-FeCSiMn hardness and Young's moduli for compression stresses

Unit/method	Mean hardness	Hardness deviation	Mean Young's modulus	Young's modulus deviation
Macroindentation into coating surface				
HRC	27.6	1.0		
HV30	307	14		
HBW 1.5875/50	228	27		
HBW 1.5875/40	180	10		
HBW 1.5875/30	171	31		
HBW 1.5875/20	147	2		
HBW 1.5875/16.625	172	15		
HBW 1.5875/10	161	13		
HBW 1.5875/5	128	9		
Microindentation into coating surface				
HV1	405	71		
HV0.1	604	124		
GPa (NanoIndent, 500 nm)	5.3	2.4	127	59
GPa (NanoIndent, 250 nm)	6.3	2.3	142	37
GPa (NanoIndent, 100 nm)	6.9	2.8	154	34
Microindentation in cross section				
HV1	466	91		
HV0.1	625	112		
GPa (NanoIndent, 500 nm)	8.2	2.3	165	31
GPa (NanoIndent, 250 nm)	11.3	4.2	203	52
GPa (NanoIndent, 100 nm)	13.8	4.5	240	70

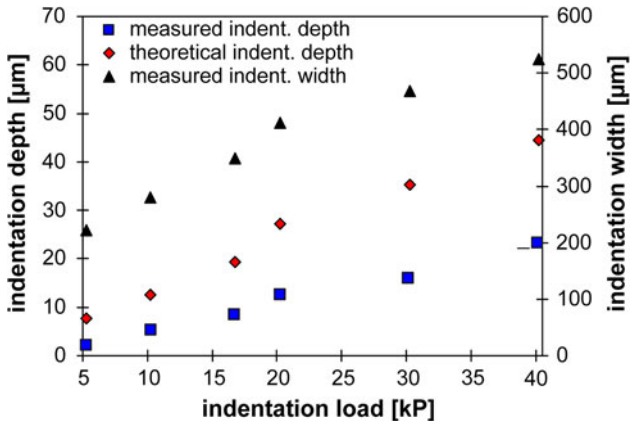

Fig. 8 Indentation test results of WC-FeCSiMn employing Ø 1.5875 mm WC-Co spherical indenter

However, the Young's modulus could be evaluated by nanoindentation experiments. In combination with SEM validations of the imprints, valuable results were generated for indentations into the surface and the cross section. Mean values were calculated for each indentation depth, excluding indentations into coating pores, voids, or microcracks (Table 3).

Concerning the anisotropy of the lamellar layer with elongated splats perpendicular to the spray direction, the hardness and Young's modulus values were determined to be larger in the cross section of the coating than at its surface. Figure 9 exemplarily shows the interaction of two cross-section indentation imprints with the microstructure of the coating. Single material phases can be hit with an imprint diameter of approximately 2.5 µm for 500 nm indentations (Fig. 9a). Thus, a huge influence of splat interfaces and coterminous phases is given. The lower the indentation depth is, the higher is the probability to hit

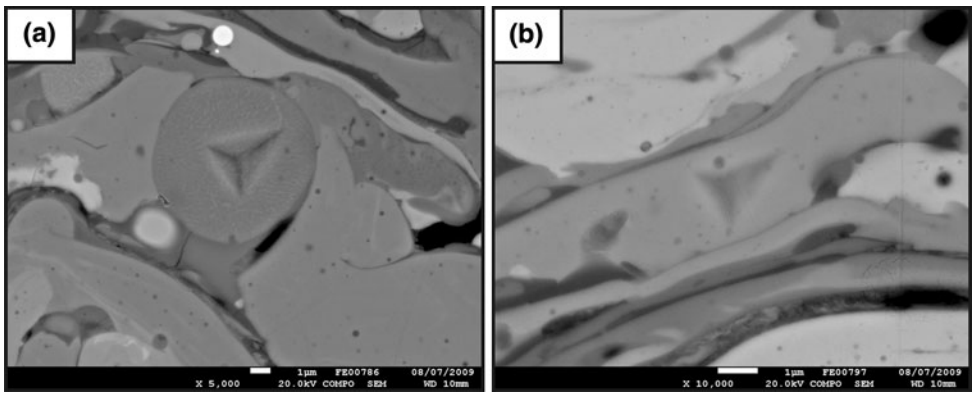

Fig. 9 SEM micrographs of nanoindentation imprints into the coating cross section (backscattering mode). (a) 500 nm imprint into spherical coating inclusion containing mainly FeCSiMn. (b) 250 nm imprint into pseudoalloyed WC-FeCSiMn phase

only one single material phase. Additionally, the influence of the interface decreases. However, higher deviations between the measurements of load-displacement curves can be detected at lower loads (Table 3). This is due to the higher relevance of the elementary phase composition at the very local imprint of the Berkovich indenter. Investigations of SEM micrographs show that phases of different compositions can be identified because of the material contrast in the backscattering mode of the SEM. However, it has to be mentioned that neither with the backscattering mode nor with EDS quantitative separations between WC and W_2C could be achieved. Furthermore, the resolution of the WC-FeCSiMn pseudoalloyed phase composition EDS measurements is restricted and includes some of the interface around the imprints.

Some further details are given in the paper of Tillmann et al. (Ref 50), which concerns with the simulation of micro- and macroscopic WC-FeCSiMn coating behaviors under compressive loads on the basis of the same nanoindentation experiments.

3.4 Bending Test

According to Eq 3-5, stress-strain curves, bending strength, and Young's modulus were determined for the freestanding WC-FeCSiMn coatings (Fig. 10). The curve progression shows the characteristic linear behavior of brittle materials just below the point where failure occurs.

Stated at assessed values of bending, the freestanding coatings the mean bending strength was determined to be 203 ± 26 N/mm^2. The Young's modulus under bending stress was calculated to be 64.6 ± 4.5 GPa for the tested samples. As an interesting result, the Young's modulus determined in the bending tests is about 60% lower compared with the mean compressive Young's modulus measured by nanoindentation. This characteristic goes along with the results of Kim and Kweon (Ref 20) describing this effect for plasma sprayed $MgZrO_3$-35NiCr, Al_2O_3-30(Ni20Al), and (ZrO_2-24MgO)-35(Ni20Cr6Al) cermet coatings. Moreover, his experiments showed significant lower Young's modulus values determined in three-point bending tests when compared with Knoop indentation experiments (Ref 20). One of the reasons for this is that the indentation test measures the near-intrinsic property of materials due to the limited test volume, while tension and bending tests include extrinsic microstructural characteristics such as pores and microcracking (Ref 20). Furthermore, to determine the Young's modulus of the material, the Knoop or nanoindentation experiment considers only an elastic response after the unloading cycle. However, the bending and tensile tests include inelastic features such as microcracking, splat boundary sliding, and pore deformation.

However, the difference between the measured compressive and tensile behavior of the inhomogeneous coating is not a complete error in the measurement. Rather, the inhomogeneous layer shows more resistance to compressive loads, as the sliding of the splat boundaries and microcracks are restricted considerably.

In contrast to the sensible results obtained for the freestanding coatings, the bending tests of coated steel specimens attained unreliable values. Because of undefined interactions of the grit-blasted substrate surface and the rough coating bottom, the testing of several identical specimens resulted in distinctly divergent calculated bending stresses and Young's moduli. Because of considerably lower yield strengths compared with the steel substrate as well as the potential of hidden microcracking in the coating, the bending strength could not be determined for the steel-coating compound. However, the brittle fracture mechanics could be analyzed by microscopy of the cracked cross section (Fig. 11).

The SEM investigation revealed the brittle character of the WC-FeCSiMn coating. Stressed by tensile strains, the layer showed cracking without any plastic deformation (Fig. 11). Therefore, it seems to be possible to reassemble the two broken parts of the coating to reproduce the original shape. The crack propagation is mainly affected by forced fracture from one lamella to the next using the weak points (precracks, pores) in the layer. However,

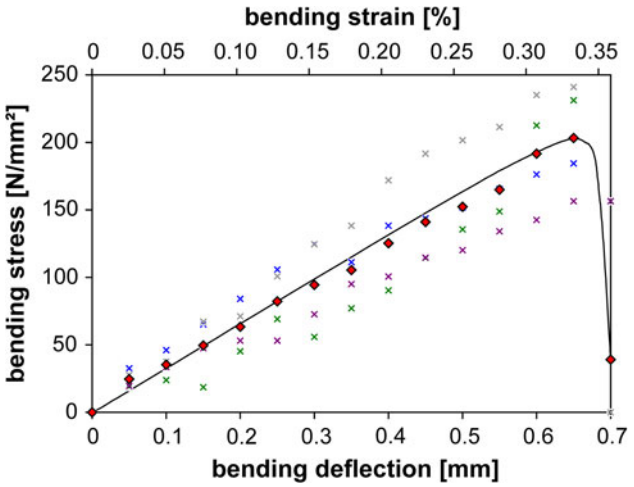

Fig. 10 Stress-strain curves for five freestanding WC-FeCSiMn coatings measured in bending tests

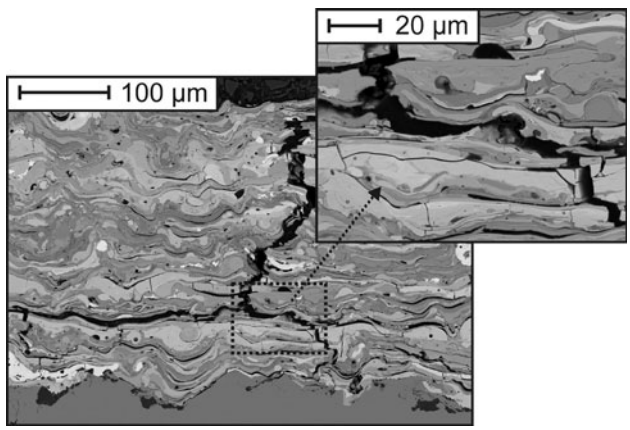

Fig. 11 SEM cross section of crack propagation after bending (tensile strain)—TWAS WC-FeCSiMn on steel

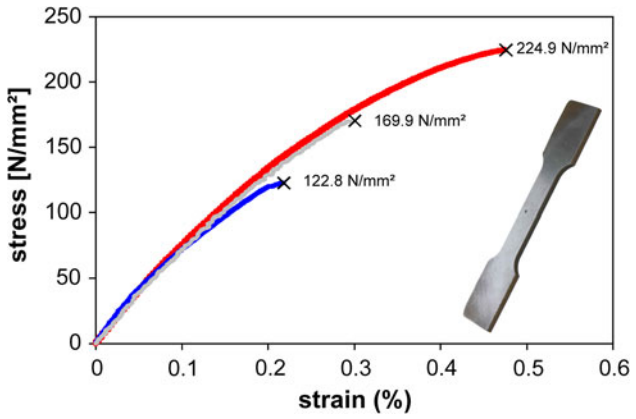

Fig. 12 Stress-strain curves for three freestanding WC-FeCSiMn coatings measured in tensile tests

because the fracture direction is mainly perpendicular to the bending stress a number of horizontal cracks between the splats are visible, indicating stress relaxation by the delamination of weak splat boundaries.

3.5 Tensile Tests

Hence, it was determined in the bending experiments that it was not possible to identify the coating properties on steel-coating compounds by tensile tests. The influence of the undefined interaction of substrate and coating is too high. It could be assumed that especially the roughness of the grit-blasted substrate causes a transmission of the one-directional strain of the tension test to an irregular three-dimensional stress field. Testing of several identically coated specimens resulted in different stress-strain curves. The unknown stress distribution in the mechanically bonded substrate-coating compound prevents the calculation of reliable values of tensile strength and Young's modulus. As in the bending experiment, only the fracture pattern could be investigated on the material compound.

However, three sensible stress-strain curves were determined for spark-eroded freestanding coatings (Fig. 12).

Due to the brittle character of the coating, the stress-strain curves of WC-FeCSiMn do not have a yield point. The ultimate strength and breaking strength are the same. Nevertheless, different failure stresses were observed for each sample, which is characteristic for materials failing while the deformation is mainly elastic. Just a small amount of ductile behavior was determined for the coating before breaking.

The Young's modulus under tensile load was calculated to be 81.5 ± 4.7 GPa which is in good correlation with the bending test results.

4. Conclusion

In this study, TWAS sprayed WC-FeCSiMn coatings are evaluated. Supplementary to previous published works concerning the spraying parameter optimization, microstructure, porosity, hardness, and wear resistance (Ref 40-42) the focus of this paper is on the compression, bending, and tensile behavior of the coating.

The compression behavior of the coating was investigated by hardness Vickers, Brinell, Rockwell, and nanoindentation experiments. All investigated indentation tests confirmed that the cross-section hardness of the coating is higher than the hardness measured on the polished coating surface correlating with the anisotropic microstructure of the layer. Additionally, a strong correlation between indentation load and hardness of the coating was recognized. Much more distinctive than for bulk materials, the effect showed increased hardness values for decreased loads regarding the inhomogeneous microstructure of the lamellar coating, including microcracks, pores, and weak interface boundaries between splats.

Though the investigation of the compressive strength and Young's modulus using spherical indentation was not successful, the measurements contributed detailed information about the forming behavior of the TWAS WC-FeCSiMn coating under pointed loads. Due to the anisotropy of the lamellar layer, the pointed stress under the indenter tip is noticeably transferred parallel to the splat expansion direction. This directed stress propagation results in wider indentation diameters for spherical indenter impressions.

Verified values for the elastic and plastic properties of the coating under compression loads were determined by nanoindentation measurements. Batches of each 49 indents were investigated for 100, 250, and 500 nm indentations into the surface as well as into the cross section of the coating. Their validity was determined by SEM. Mean hardness values and Young's moduli were calculated after excluding indentations into pores, voids, or microcracks.

Increased hardnesses and Young's moduli were measured for decreased loads. Additionally, higher values than those for indentations into the surface were confirmed for the cross section of the coating. However, the inhomogeneity of the arc sprayed layer featuring different phase compositions and weak splat boundaries (interface) resulted in high scattering of the nanoindentation measurements.

For tensile loads, bending and tensile test generated valuable and comparable results. It was revealed that the elongation of TWAS sprayed WC-FeCSiMn under tension load is limited to a maximum strain of 0.45%. Due to the brittle character of the WC-FeCSiMn coating the stress-strain curves do not have a yield point. Since the deformation is dominated by elastic strain, plastic deformations are almost absent. The ultimate and breaking strength are the same. Failure in the form of brittle fracture appears more or less without premonition. Correlating with the brittle character of the cermet coating, a significant difference was observed between compression and tensile behavior. Hence, the Young's modulus for the tension case is about 60% lower than for the compression case. This is mainly due to three effects:

(1) The bending and tensile tests are sensitive to pre-cracks, weak splat boundaries, or pores. At tensile or

shear loads, sliding of broken parts or boundaries can occur easily. However, under compressive loads, even phases and lamellae with microcracks or weak bonding can show remarkable resistance.

(2) Tensile tests and bending tests only evaluate the weakest point of the material compound, for example, the position with most defects. On the contrary, indentation tests only evaluate the selected, local position.

(3) Due to the fast cooling of the molten spraying particles at their impact on the substrate, residual tensile stresses are induced into the layer. These residual tensile stresses lead to a lower ultimate strength of the sprayed coating, which can lead to premature cracking and failure within some of the layer lamellae.

Acknowledgments

This work was supported by the German Research Foundation (DFG) within the SFB 708. In addition to this financial promotion, the authors would like to thank W. Piotrowski, V. Brandt, J. Vahrenholt, and B. Klusemann for their assistance conducting the spraying experiments, metallography, porosity measurements, and mechanical testing. Special thanks to R. Zarnetta (Institute of Materials, Ruhr University Bochum) for his support realizing the nanoindentation experiments.

References

1. B. Wielage, S. Steinhäuser, and M. Wözel, Untersuchungen zum Einfluss der Prüfbedingungen auf die Prüfergebnisse bei Verschleißuntersuchungen an thermisch gespritzten WC-Co-Schichten mit dem Taber-Abraser, Tribologie-Fachtagung 2002-2, Göttingen, Germany, 2002, p 68/1-68/13 (in German)
2. E. Lugscheider and C. Herbst, Thermisch gespritzte Verschleißschutzschichten heute und morgen, *Pulvermetallurgie in Wissenschaft und Praxis,* Vol 13, DGM-Informationsgesellschaft, Oberursel, Germany, 1997, p 163-188 (in German)
3. B. Wielage, H. Pokhmurska, A. Wank, G. Reisel, et al., Influence of Thermal Spraying Method on the Properties of Tungsten Carbide Coatings, *Proceedings of the Conference on Modern Wear and Corrosion Resistant Coatings Obtained by Thermal Spraying*, Nov 20-21, 2003 (Warsaw, Poland), 2003, p 39-48
4. K. Smolka, *Thermisches Spritzen. Ein Leitfaden für den Praktiker*, Vol 15, DVS Deutscher Verlag für Schweißtechnik, Düsseldorf, Germany, 1985, 105 p (in German)
5. S. Siegmann and O. Brandt, ''Thermally Sprayed Protection Coatings with Highest Resistance against Wear and Corrosion, Made by Nanostructured Powders,'' PPM—Swiss Priority Program on Materials Research, Final Report, 2000, p 201-216
6. R.T.R. McGrann, D.J. Greving, J.R. Shadley, E.F. Rybicki, B.E. Bodger, and D.A. Somerville, The Effect of Residual Stress in HVOF Tungsten Carbide Coatings on the Fatigue Life in Bending of Thermal Spray Coated Aluminum, *J. Therm. Spray Technol.*, 1998, **7**(4), p 546-552
7. Z. Yin, S. Tao, X. Zhou, and C. Ding, Evaluating Bending Strength of Plasma Sprayed Al_2O_3 Coatings, *J. Therm. Spray Technol.*, 2009, **18**(2), p 292-296
8. H. Brantner, R. Pippan, and W. Prantl, Local and Global Fracture Toughness of a Flame Sprayed Molybdenum Coating, *J. Therm. Spray Technol.*, 2003, **12**(4), p 560-571
9. S. Houdkova, R. Enzl, F. Zahalka, and O. Blahova, The Indentation Tests for Evaluation of HVOF Coatings' Mechanical Properties, *International Thermal Spray Conference: Explore its Surfacing Potential,* E. Lugscheider, Ed., May 2-4, 2005 (Basel, Switzerland), DVS Deutscher Verband für Schweißen, 2005, p 1-5
10. A. Gouldstone, N. Chollacoop, M. Dao, J. Li, A.M. Minor, and Y.L. Shen, Indentation Across Size Scales and Disciplines: Recent Developments in Experimentation and Modeling, *Acta Mater.*, 2007, **55**(12), p 4015-4039
11. L. Barbieri, G. Bolelli, V. Cannillo, L. Lusvarghi, and S. Riccò, Computational Simulations and Experimental Characterization of the Mechanical and Fracture Behaviour of Alumina-Glass Plasma Sprayed Coatings, *International Thermal Spray Conference: Explore its Surfacing Potential,* E. Lugscheider, Ed., May 2-4, 2005 (Basel, Switzerland), DVS Deutscher Verband für Schweißen, 2005, p 1-6
12. M. Factor and I. Roman, Microhardness as a Simple Means of Estimating Relative Wear Resistance of Carbide Thermal Spray Coatings: Part 1 Characterization of Cemented Carbide Coatings, *J. Therm. Spray Technol.*, 2002, **11**(4), p 468-481
13. M. Factor and I. Roman, Use of Microhardness as a Simple Means of Estimating Relative Wear Resistance of Carbide Thermal Spray Coatings: Part 2. Wear Resistance of Cemented Carbide Coatings, *J. Therm. Spray Technol.*, 2002, **11**(4), p 482-495
14. A. Ibrahim, R.S. Lima, B.R. Marple, and C.C. Berndt, Fatigue and Mechanical Properties of Nanostructured vs. Conventional Titania (TiO_2) Coatings, *International Thermal Spray Conference: Explore Its Surfacing Potential,* E. Lugscheider, Ed., May 2-4, 2005 (Basel, Switzerland), DVS Deutscher Verband für Schweißen, 2005, p 1-5
15. M.A. Camerucci, G. Urretavizcaya, and A.L. Cavalieri, Mechanical Behavior of Cordierite and Cordierite-Mullite Materials Evaluated by Indentation Techniques, *J. Eur. Ceram. Soc.*, 2001, **21**, p 1195-1204
16. R. Lima, S. Kruger, G. Lamouche, and B. Marple, Elastic Modulus Measurements via Laser-Ultrasonic and Knoop Indentation Techniques in Thermally Sprayed Coatings, *J. Therm. Spray Technol.*, 2005, **14**(1), p 52-60
17. J. Li and C. Ding, Determining Microhardness and Elastic Modulus of Plasma-Sprayed Cr_3C_2-NiCr Coatings Using Knoop Indentation Testing, *Surf. Coat. Technol.*, 2001, **135**(2-3), p 229-237
18. J. Gong, Z. Zhao, Y. Yang, Z. Guan, and H. Miao, Statistical Variability in the Indentation Toughness of TiCN Particle Reinforced Al_2O_3 Composite, *Mater. Lett.*, 2001, **49**, p 357-360
19. D.B. Marshall, T. Noma, and A.G. Evans, Simple Method for Determining Elastic-Modulus-to-Hardness Ratios Using Knoop Indentation Measurements, *J. Eur. Ceram. Soc.*, 1982, **65**(10), p 175-176
20. H.-J. Kim and Y.-G. Kweon, Elastic Modulus of Plasma-Sprayed Coatings Determined by Indentation and Bend Tests, *Thin Solid Films*, 1999, **342**(1-2), p 201-206
21. E.G. Herbert, G.M. Pharr, W.C. Oliver, B.N. Lucas, and J.L. Hay, On the Measurement of Stress-Strain Curves by Spherical Indentation, *Thin Solid Films*, 2001, **398-399**, p 331-335
22. W.C. Oliver and G.M. Pharr, An Improved Technique for Determining Hardness and Elastic Modulus Using Load and Displacement Sensing Indentation Experiments, *J. Mater. Res.*, 1992, **7**(6), p 1564-1583
23. J. Gong, H. Miao, and Z. Peng, A New Function for the Description of the Nanoindentation Unloading Data. Viewpoint Set No. 30. Mechanical Properties of Quasicrystals, *Scr. Mater.*, 2003, **49**(1), p 93-97
24. J. Gong, H. Miao, and Z. Peng, Analysis of the Nanoindentation Data Measured with a Berkovich Indenter for Brittle Materials: Effect of the Residual Contact Stress, *Acta Mater.*, 2004, **52**(3), p 785-793
25. D. Ma, C.W. Ong, and T. Zhang, An Instrumented Indentation Method for Young's Modulus Measurement with Accuracy Estimation, *Exp. Mech.*, 2009, **49**(5), p 719-729
26. P.L. Larsson, A.E. Giannakopoulos, E. Söderlund, D.J. Rowcliffe, and R. Vestergaard, Analysis of Berkovich Indentation, *Int. J. Solids Struct.*, 1996, **33**(2), p 221-248

27. J. Tan, P.J. Meadows, D. Zhang, X. Chen, E. López-Honorato, X. Zhao et al., Young's Modulus Measurements of SiC Coatings on Spherical Particles by Using Nanoindentation, *J. Nucl. Mater.*, 2009, **393**(1), p 22-29
28. M. Dao, N. Chollacoop, K.J. van Vliet, T.A. Venkatesh, and S. Suresh, Computational Modeling of the Forward and Reverse Problems in Instrumented Sharp Indentation, *Acta Mater.*, 2001, **49**(19), p 3899-3918
29. S.V. Hainsworth, H.W. Chandler, and T.F. Page, Analysis of Nanoindentation Load-Displacement Loading Curves, *J. Mater. Res.*, 1996, **11**(8), p 1987-1995
30. R.W. Hertzberg, *Deformation and Fracture Mechanics of Engineering Materials*, 4th ed., John Wiley & Sons, Chichester, 1995, 816 p
31. S. Okamoto, Y. Nakazono, K. Otsuka, Y. Shimoitani, and J. Takada, Mechanical Properties of WC/Co Cemented Carbide with Larger WC Grain Size, *Mater. Charact.*, 2005, **55**(4-5), p 281-287
32. Y. Podrezov, Y. Mil'man, D. Lotsko, N. Lugovoi, D. Verbilo, and N. Efimov, A Method of Determining the Mechanical Properties of a Two-Layer Composite Consisting of a Steel Matrix, a Plasma Spray Coating Based on Amorphizing Powders, *Powder Metall. Met. Ceram.*, 1999, **38**(5), p 224-227
33. N.A. Dolgov, Method for Determining the Modulus of Elasticity for Gas Thermal Spray Coatings, *Powder Metall. Met. Ceram.*, 2004, **43**(7-8), p 423-428
34. R.F. Bunshah, *Handbook of Hard Coatings: Deposition Technologies, Properties and Applications*, Noyes Publications, Park Ridge, NJ, 2001, 550 p
35. S. Bouaricha, J.-G. Legoux, and P. Marcoux, Bending Behavior of HVOF Produced WC-17Co Coating: Investigated by Acoustic Emission, *J. Therm. Spray Technol.*, 2004, **13**(3), p 405-414
36. DIN EN 843/1-6, "Hochleistungskeramik—Mechanische Eigenschaften monolithischer Keramik bei Raumtemperatur" (Advanced Technical Ceramics—Mechanical Properties of Monolithic Ceramics at Room Temperature), Deutsches Institut für Normung, 2007, 182 p (in German)
37. DIN EN ISO 6892/1-2, "Metallic Materials—Tensile Testing," International Organization for Standardization, 2009, 92 p
38. A. Koutsomichalis, N. Vaxevanidis, G. Petropoulos, A. Mourlas, and S. Antoniou, Friction, Wear and Mechanical Behaviour of Plasma Sprayed WC-12% Co Coatings on Mild Steel, *THE Coatings 2008, Proceedings of the Seventh International Conference,* Oct 1-3, 2008 (Chalkidiki, Greece), 2008, p 259-268
39. J. Voyer and H. Kreye, Determination of Cracking Resistance of Thermal Spray Coatings During Four-Point Bend Testing Using an Acoustic Emission Technique, *J. Therm. Spray Technol.*, 2003, **12**(3), p 416-426
40. W. Tillmann, E. Vogli, I. Baumann, B. Krebs, and J. Nebel, Thermally Sprayed Wear-Protective Cermet Coatings for Forming Tools, *The Fourth International Conference on Spray Deposition and Melt Atomization, SDMA 2009*, Sept 7-9, 2009 (Bremen, Germany), 2009
41. W. Tillmann, E. Vogli, and J. Nebel, Einfluss der Spritzparameter auf die mechanischen und tribologischen Eigenschaften von lichtbogengespritzten WSC-FeCSiMn Schichten (Influence of Coating Parameters on the Mechanical and Tribological Properties of Arc-Sprayed WSC-FeCSiMn Coatings), SFB 708-3, öffentliches Kolloquium, Nov 25, 2009 (Dortmund, Germany), p 141-152 (in German)
42. W. Tillmann, E. Vogli, I. Baumann, B. Krebs, and J. Nebel, Wear-Protective Cermet Coatings for Forming Tools/Cermet-Schichten für den Verschleißschutz von Umformwerkzeugen, *Materialwiss. Werkstofftech.*, 2010, **41**(7), p 597-607
43. ASTM Standard E837, *Standard Test Method for Determining Residual Stresses by the Hole-Drilling Strain-Gage Method*, ASTM International, West Conshohocken, PA, 2008, 17 p
44. DIN EN ISO 6506/1-4, "Metallische Werkstoffe—Härteprüfung nach Brinell" (Metallic Materials—Brinell Hardness Test), Deutsches Institut für Normung, 2006, 63 p (in German)
45. DIN EN ISO 6507/1-4, "Metallische Werkstoffe—Härteprüfung nach Vickers" (Metallic Materials—Vickers Hardness Test), Deutsches Institut für Normung, 2006, 148 p (in German)
46. DIN EN ISO 6508/1-3, "Metallische Werkstoffe—Härteprüfung nach Rockwell" (Metallic Materials—Rockwell Hardness Test), Deutsches Institut für Normung, 2006, 63 p (in German)
47. VDI/VDE 2616/1, "Hardness Testing of Metallic Materials," Verein Deutscher Ingenieure, Verband der Elektrotechnik, Elektronik, Informationstechnik, 2002, 52 p
48. DIN EN ISO 4516, "Metallische und andere anorganische Überzüge—Mikrohärteprüfungen nach Vickers und Knoop" (Metallic and Other Inorganic Coatings—Vickers and Knoop Microhardness Tests), Deutsches Institut für Normung, 2002, 16 p (in German)
49. B.R. Lawn, Indentation of Ceramics with Spheres: A Century after Hertz, *J. Am. Ceram. Soc.*, 1998, **81**(8), p 1977-1994
50. W. Tillmann, B. Klusemann, J. Nebel and B. Svendsen, Analysis of the Mechanical Properties of an Arc-Sprayed WC-FeCSiMn Coating: Nanoindentation and Simulation, *J. Therm. Spray Technol.*, 8 p, doi:10.1007/s11666-010-9550-8